11th Australasian Fluid Mechanics Conference
University of Tasmania, Hobart, Australia
14-18 December 1992

SOME ASPECTS OF THE EFFECTS OF STREAMLINE CONVERGENCE ON A FULLY DEVELOPED TURBULENT BOUNDARY LAYER

Salah HAFEZ and Peter N. JOUBERT

Department of Mechanical & Manufacturing Engineering
University of Melbourne, Parkville, VIC 3052
AUSTRALIA

ABSTRACT

An experimental study which examines the response of a fully developed turbulent boundary layer to the application and removal of a prolonged streamline convergence is presented. The convergence is of the type created by sink flow over a flat plate. Preliminary analysis of the results indicates that convergence of streamlines leads to a very rapid thickening of the boundary layer and to an increase of the broad-band turbulence and Reynolds shear stress quantities in the outer layer. This is followed by a reduction of the rate of growth of the layer and the turbulence quantities leading to the formation of an internal layer.

INTRODUCTION

The development of boundary layers over complex surfaces, such as ship hulls, are affected by the complexities of the three-dimensional shapes. These complex effects are called extra-rates-of-strain (see Bradshaw, 1973). These are introduced into the flow by surface curvature, pressure gradients, lateral straining, etc. The difficulty with complex flows arises from the non-linear effects which the extra-strain rates have on the turbulence structure. Due to these extra-strain rates, the Reynolds transport equations for zero-pressure-gradient plane parallel-flow turbulent boundary layers are modified and extra explicit terms appear in the equations, but the effects of the extra-strain rates are generally one order of magnitude higher than these extra terms. The existing prediction methods cannot fully predict these flows as pointed out by Bradshaw (1988). This is true when a combination of the extra-strain rates affects the boundary layer. The total effects on the boundary layer cannot be considered as a linear summation of each individual effect (see Smith and Wood, 1985). Consequently, in order to aid and improve our prediction capabilities of the complex flows, we have to resort to experimentation. The extra-strain rate due to lateral straining is equal to $\partial W/\partial z$ (Cartesian coordinate system is used: x-axis along the flow direction, y-axis normal to the wall and z-axis in spanwise direction. The respective mean components of the velocity in these directions are U, V and W, and the fluctuating components are u, v and w. Overbars denote time averages). As well as other extra rates of strain, the boundary layers over the nose and tail of a body of revolution are affected by streamline divergence ($\partial W/\partial z > 0$) and streamline convergence ($\partial W/\partial z < 0$) respectively. Recently, the first stage of the experimental studies into the effects of lateral straining was completed. For that study a specially-designed wind tunnel was built to examine the effects of "simple" streamline divergence on developing turbulent boundary layers. By the term "simple" it is meant that the divergence remains constant through the boundary layer (e.g. flow over cone and source flow over flat plate), however, when the divergence increases from the edge of the boundary layer to the wall (e.g. the divergence occurring on the attachment line of a swept wing), it is known as the "varying" type (Head and Prahlad, 1974). The effects of streamlines divergence were studied in details at low Reynolds number and reported by Saddoughi and Joubert (1991). It appears that there are two other experiments which dealt with the study of streamline convergence. Both these experiments were of the type of sink flow over a flat plate. Sjolander (1980) took only mean-flow measurements for both "varying" and "simple" convergence cases in the presence of a pressure gradient. Crabbe (1977) presented limited turbulence measurements for the effects of "varying" convergence on a boundary layer. No study exists in the literature for the relaxation from the converging streamlines which is another aspect to investigate within this study. Initial measurementss with different instrumentation were taken and reported by Saddoughi et al. (1991). The present measurements and analysis are slightly different, but consistent with the earlier one.

APPARATUS AND TECHNIQUES

The experiment was conducted in an open-return blower wind tunnel. The working section measured 610 x 310 mm after the exit from a 6:1 three dimensional contraction. Measurements were carried out at a constant unit Reynolds number (1.3×10^6 m^{-1}) which corresponds to a nominal reference velocity, U_R, of 20 m/s. A 0.5 mm trip wire was used to trip the boundary layer on one of the vertical walls forming the working section. The layer was allowed to develop in a straight walled section for a distance about 2 m. Simple convergence was achieved by tilting two straight side walls, initially in a horizontal position. The total included angle was 20^0 and extended for 800 mm in the streamwise direction. The pressure gradient for the boundary layer was controlled by flexible walls opposite to the one over which the boundary layer developed. The flexible walls with two bleeding slots, found by trials, were found to produce the least change of pressure in the streamwise direction, as shown in Fig. 1. Due to the changes of the side wall orientation from straight to inclined and back to straight again the streamwise pressure gradient was not zero over the entire working section after the application of the convergence. It is clear that the region where the relaxation takes place, $x > 800$ mm, will be most affected by the present streamwise pressure gradient. Spanwise pressure coefficient distributions are given in Fig. 2 for the stations which showed significant pressure gradient. Mean flow velocity traverses were measured by a 0.73 mm o.d. total head Pitot tube. The static pressure was measured by another tube placed about 25 mm above the total head tube. Local values of skin friction coefficient were deduced from the measured velocity profiles by fitting the central part to a log-law with constants $\kappa = 0.41$ and $C = 5.0$. It is shown by Head and Prahlad (1974) that for small values of convergence angles, the lateral strain rate, $\partial W/\partial z$, is equal to UD, where D is the convergence. Its value at any point on the plane of symmetry of the flow is equal to $1/(x - x_0)$, where x_0 is the distance from the start of the converging section to the virtual origin of convergence.The convergence parameter is defined as $e/(\partial U/\partial y)$, where $e = \partial W/\partial z$. The design value of

convergence will be used to calculate the convergence parameter at the mid point of the layer. Mean flow length scales such as the displacement thickness, δ^*, and momentum thickness, θ, were calculated from the mean flow velocity profiles measured with the pressure probe. Knowledge of the boundary layer length scale is important in order to analyse both the mean flow in the velocity defect form and the broad-band turbulence intensities with outer flow scaling. The commonly used boundary layer thickness, e.g. $\delta_{0.99}$ or $\delta_{0.995}$, are very sensitive to inaccuracies in velocity measurements at the outer edge of the layer. A better defined thickness δ_H, the Hama boundary layer thickness, will be used
i.e.

$$\delta_H = (\delta^* U_e)/(C_1 U_\tau) \quad (1)$$

where $C_1 = \int (U_e - U)/U_\tau \, d\eta$; $0 \le \eta \le 1$ and $\eta = y/\delta_H$ (2)

Hama (1954) defined this only for zero pressure gradient layers but its use can be generalized. It is clear that (2) depends on the proper representation of the velocity profile and mostly on the Coles wake function, W_c. The polynomial formula for the Coles wake function due to Lewkowicz (1982) was used. This formula can be written as follows :

$$W_c[\eta, \Pi] = 2\eta^2 (3 - 2\eta) - \eta^2/\Pi(1 - \eta)(1 - 2\eta) \quad (3).$$

By employing (3) with a logarithmic velocity profile to represent the mean flow velocity profile, for $y^+ > 50$, the value of C_1 is found to be

$$C_1 = 1/\kappa (\Pi + 59/60) + 60/K_\tau \quad (4)$$

where K_τ is the karman number, $\delta_H U_\tau/\nu$, and $y^+ = y U_\tau/\nu$.

The friction velocity is U_τ, and ν is the kinematic viscosity.

The last term in (4) introduces the Reynolds number effect by employing universal integrals for the near-wall velocities as substitute for the near-wall velocity measurements in the calculation of integral length scales for $y^+ < 50$ (see Coles, 1968). Normal and crossed wire measurements for broad band turbulence quantities were taken. The normal (single-sensor DISA 55 P05) and crossed (dual-sensor DISA 55 P51) hot wires were used with constant temperature anemometers designed at the University of Melbourne (see Perry and Morrison 1971a). Wollaston wires were soldered to the probe and etched to give a filament of 5μm platinum cores and active lengths ≈1.0 mm. The crossed wires were nominally at $\pm 45^0$ to the mean flow direction and the probe could be rotated accurately about its axis through 90^0, enabling measurements in two perpendicular planes (referred to as the ' UV' mode and 'UW' mode) to be made at a point. Broad band turbulence quantities were measured with calibrated wires using the dynamic calibration technique developed by Perry and Morrison (1971b) and detailed by Perry (1982). The signals from the crossed wires were electronically matched using a specially designed matching box (for details see Perry, 1982). Signals were sampled on line with a 32 bit 386-IBM compatible personal computer using Analogue-Devices RTI 860 data acquisition board. Broad band turbulence measurements were taken in a burst of 8000 samples and 5 bursts were sufficient to have results converged within 1%. The streamwise broad-band turbulence intensity at the reference station, x= -250 mm, measured using different techniques, is displayed in figure 3. The agreement is good and gives some credibility to the measuring techniques and the following results.

RESULTS AND DISCUSSION

Measurements were carried out at ten stations along the plane of symmetry of the boundary layer. Due to the limited space of this paper, only data collected within the converging section will be presented. The locations of these stations and the reduced mean flow parameters such as the Reynolds number based on the momentum thickness R_θ, the Coles wake factor Π, the shape parameter H, skin friction coefficient C_f, in addition to other details are given in Table I.

TABLE I : Mean flow parameters

x(mm)	-250	40	200	360	610	790
R_θ	4446	5510	6574	8306	11462	13783
K_τ	1670	2011	2303	2603	3146	3893
$e/(\partial U/\partial y)$		-.054	-.065	-.085	-.128	-.187
Π	0.59	0.64	0.70	0.85	1.13	1.13
H	1.405	1.398	1.397	1.399	1.413	1.404
$C_f x 10^3$	2.975	2.848	2.684	2.539	2.20	2.07
δ_H(mm)	32.60	39.83	47.42	55.94	73.99	89.72

Mean flow velocity profiles are analysed in the law of the wall plot. All profiles showed an extensive logarithmic region. The length of the logarithmic region, L, to the boundary layer thickness δ_H, at the reference station and the following two stations has a value of 0.195, which is close to the one reported by Erm and Joubert (1991) for turbulent boundary layers in zero pressure gradient with a comparable value of Π. Moving downstream this value shows a sudden drop to an average of 0.13 unto the end of the converging section. Mean velocity profiles are presented in a velocity defect plot in figure 4. It is felt that the reference station is affected by the early convergence of streamlines as shown by the deviation from the formula proposed by Hama (1954) for the zero pressure gradient turbulent boundary layer in the logarithmic wall region and shown by a solid line. Mean flow parameters at that station also differ from their expected values for a boundary layer in zero pressure gradient at similar Reynolds number, e.g. Coles (1962). The effects of convergence are felt in the first three stations as a slight increase in the velocity defect. This is followed by a large increase in the velocity defect. This large increase occurs in the measuring stations which showed a reduction in the extent of the logarithmic region. By the end of the converging section no further change can be noticed and this could be due to the weak favourable pressure gradient in that region.

Streamwise broad-band turbulence profiles, measured using a single normal wire, are given in figure 5 using inner flow scaling. Researchers have observed in zero pressure gradient turbulent boundary layers that with this type of scaling, the profiles are strongly dependent on the local value of R_θ for the range of the present data. This trend is followed in the first four measuring stations. Downstream there is an apparent sudden drop in the level of turbulence intensity in the region close to the wall followed by the appearance of a region of near constant level of turbulence. Figure 6 shows the same data but with outer flow scaling. An increase in the level of turbulence is evident and is consistent with the measuring stations especially in the outer layer. The attenuation and the presence of a region of constant level of turbulence is clear. This region is called in the literature an "internal layer" (see Smiths and Wood, 1985). The formation of such a layer appears to be following the observed distortion for the mean flow velocity profile. The normal to the wall and the spanwise broad-band turbulence intensities profiles with outer flow scaling are given in figures 7 and 8 respectively. These profiles are consistent with the picture given for the streamwise broad-band turbulence intensities and show a comparable spread in their respective turbulence intensities. In figures 9 and 10 the Reynolds shear stress profiles and the shear stress correlation coefficient, $R_{12} = -\overline{uv}/\acute{u}\,\acute{v}$, respectively are shown. The prime denotes root mean squared value for the respective quantity. The Reynolds shear stress profile at the reference station is similar to the one expected for zero pressure gradient turbulent boundary layers. The effect

of streamline convergence appears to enhance the Reynolds shear stresses before the appearance of the internal layer. The newly formed internal layer can be seen to reduce the Reynolds shear stress significantly throughout the inner half of the boundary layer and the remainder still shows an increase compared with the reference station. The Reynolds shear stress correlation coefficient displays a value ≈ 0.45 within most of the inner layer at the reference station. The effects of streamline convergence on this coefficient can be seen to enhance the mixing at the outer layer. The opposite is true for the inner layer. The extent for each region is seen to be dependent on the streamwise location after the convergence. With increasing streamwise distance the region of suppressed turbulence increases outwards.

CONCLUSIONS

Mean flow, broad-band turbulence intensities and Reynolds shear stress profiles are presented for a fully developed turbulent boundary layer subject to streamline convergence. The response of the mean flow was found to increase the value of Coles wake factor. The extent of the logarithmic region compared with the boundary layer thickness was found to drop from an initial value of ≈ 0.2 to an average value of 0.13 for the last measured stations. These observations are consistent with the changes to the broad-band turbulence intensities and Reynolds shear stress measurements. The decrease in the extent of the logarithmic region was seen as a start of an internal layer. The Reynolds shear stress correlation coefficient was found to show clearly the response of the boundary layer to the effects of the streamline convergence. It shows that streamline convergence enhances the mixing in the outer layer and reduces it in the near wall region. This leads finally to the formation of an internal layer.

ACKNOWLEDGMENT

The authors wish to thank Dr. Seyed G. Saddoughi for his help in the early stages of this investigation. This project is sponsored by the Australian Research Council.

REFERENCES

BRADSHAW, P (1973) AGARDograph 196.

BRADSHAW, P (1988) Zoran Zaric Memorial Conf. in Near-Wall Turbulence, Hemisphere Publishers.

COLES, D E (1962) Rand Rep. R-403-PR

COLES, D E (1968) AFOSR-IFP-Stanford Conference, vol. 2, ed. by Coles, Hirst.

CRABBE, R S (1977) A contribution to the study of uniformly diverging and converging turbulent boundary layers. Ph.D. dissertation, Mech. Engng., McGill University.

ERM, L P and JOUBERT, P N (1991) J. Fluid Mech. 230, 1.

HAMA, F R (1954) Soc. Naval Archit. Marine Engng., New York, Paper 6.

HEAD, M R and PRAHLAD, T S (1974) Aero. Q. 25, 293.

LEWKOWICZ, A K (1982) Z. Flugwiss. Weltraumforsch, 6, 261.

PERRY, A E (1982) Hot-Wire Anemometry , Oxford University, Clarendon press.

PERRY, A E and MORRISON, G L (1971a) J. Fluid Mech. 47, 557.

PERRY, A E and MORRISON, G L (1971b) J. Fluid Mech. 47,765.

SADDOUGHI, S G, HAFEZ, S and JOUBERT, P N (1991) 2nd Osaka Int. Colloq. on Ship Viscous flow, Osaka University and University of Osaka Prefecture.

SADDOUGHI, S G and JOUBERT, P N (1991) J. Fluid Mech. 229, 173.

SJOLANDER, S A (1980) Eddy viscosity in two-dimensional and laterally strained boundary layers. Ph.D. dissertation, University of Cambridge.

SMITS, A J and WOOD, D H (1985) Ann. Rev. Fluid Mech. 17, 312.

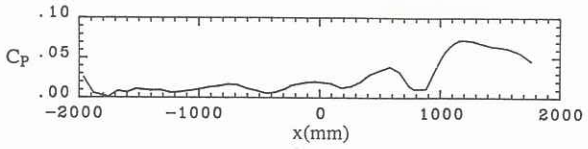

Fig. 1. Wall pressure coefficient distribution.

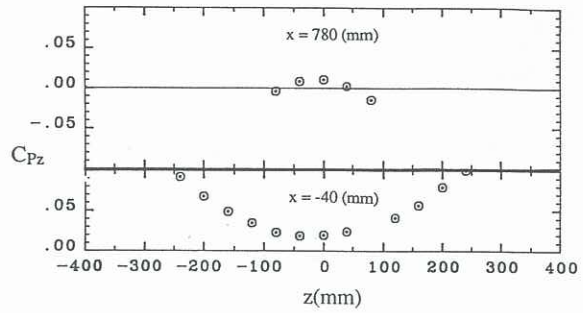

Fig. 2. Spanwise wall pressure coefficient distributions.

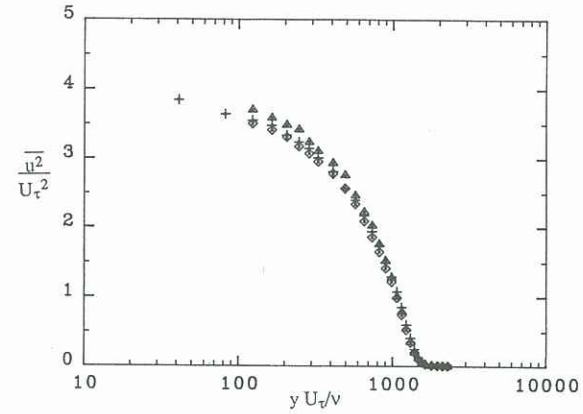

Fig. 3. Streamwise broad-band turbulence intensity with inner flow scaling at x = -250 mm :
+; normal wire, ◊; crossed wires (UV mode),
Δ; crossed wires (UW mode).

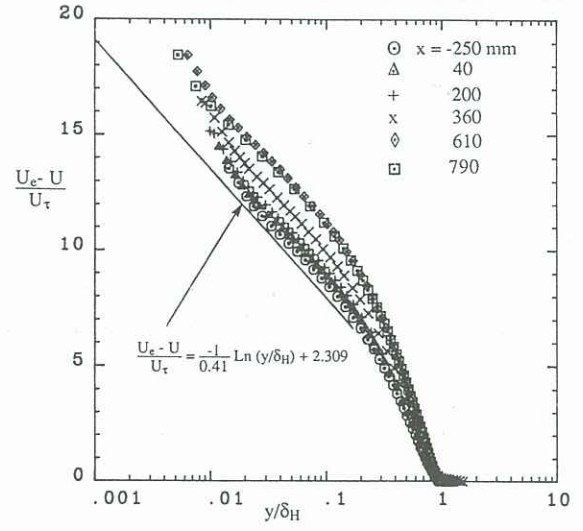

Fig. 4. Mean flow velocity defect profiles.

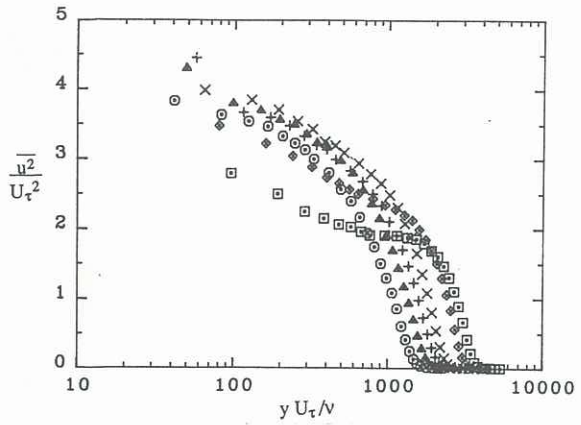

Fig. 5. Streamwise broad-band turbulence intensities with inner flow scaling. For key to symbols see figure 4.

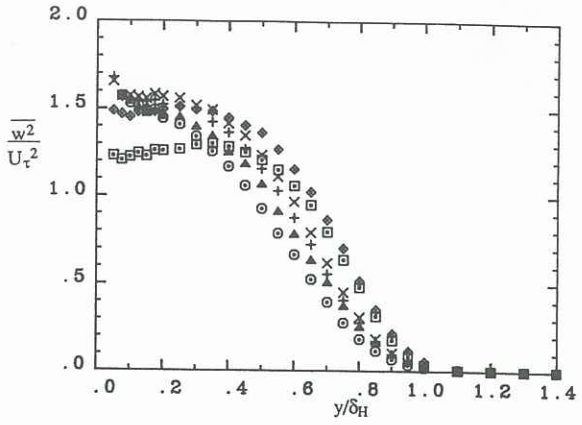

Fig. 8. Spanwise broad-band turbulence intensities with outer flow scaling. For key to symbols see figure 4.

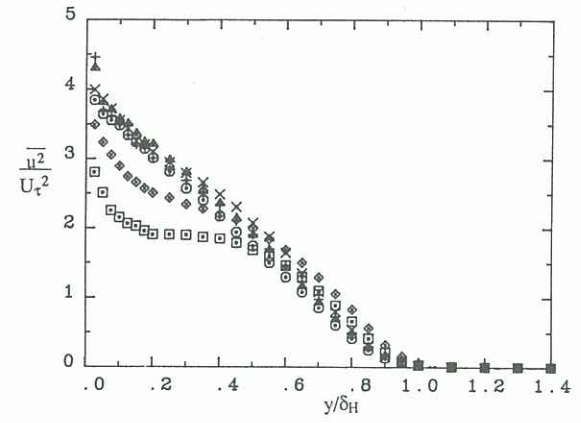

Fig. 6. Streamwise broad-band turbulence intensities with outer flow scaling. For key to symbols see figure 4.

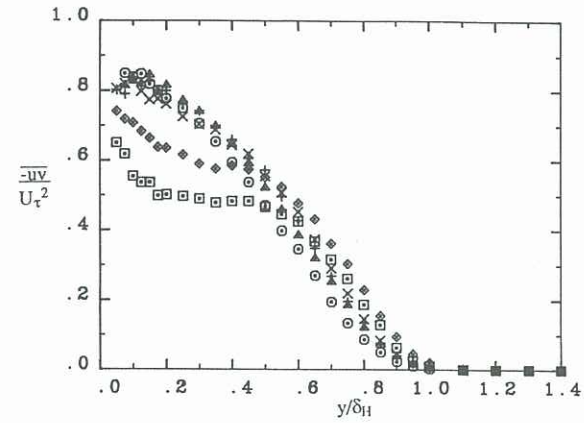

Fig. 9. Reynolds shear stresses with outer flow scaling. For key to symbols see figure 4.

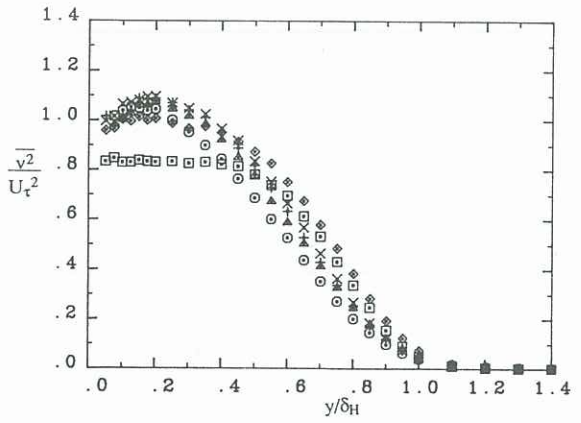

Fig. 7. Normal to the wall broad-band turbulence intensities with outer flow scaling. For key to symbols see figure 4.

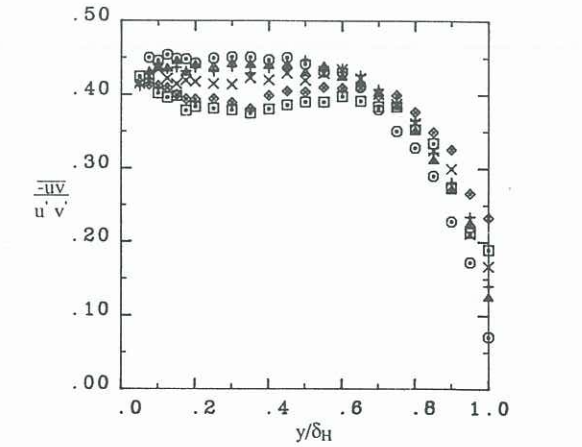

Fig. 10. Reynolds shear stress correlation coefficients with outer flow scaling. For key to symbols see figure 4.